

# Analytic Evaluation of Collocation Integrals for the Radiosity Equation.

Jaehoon Seol\*<sup>1</sup> and Kendall E. Atkinson\*\*<sup>2</sup>

<sup>1</sup> Department of Mathematics and Computer Science, Valdosta State University, 1500 N Patternson St., Valdosta, Georgia, 31698

<sup>2</sup> Department of Mathematics and Department of Computer Science, University of Iowa, Iowa City, Iowa, 52242

Received 15 November 2004, revised 30 November 2004, accepted 2 December 2004

Published online 3 December 2004

**Key words** radiosity equation, integral equation, analytic evaluation, collocation methods, computer graphics  
**AMS** 04A25

In this work, we consider solving the radiosity equation using the collocation method. We develop analytic evaluation of the integrations which are needed to setup the linear system in solving the radiosity equation using the collocation method. These integrations are over triangular elements in  $R^3$ . Our approach is to use affine transformations to convert integrations over elements in  $R^3$  to integrations over elements in  $R^2$  and then to use a change of variables. For this, we introduce functions  $H_{m,n,k}$  for  $m, n, k \in N_0$  and use these to give our analytic formulas. The analytic evaluations of  $H_{m,n,4}$  and other relevant integrations are given in detail for some values of  $m$  and  $n$ . Finally, a performance comparison of the analytic evaluation integration with that of other well-known numerical integration schemes is given.

© 2004 WILEY-VCH Verlag GmbH & Co. KGaA, Weinheim

## 1 Introduction

With the introduction of raster graphics in computer graphics, more elaborate rendering methods were needed to decide the color of all the pixels. The radiosity method was first proposed by a group of researchers at Cornell University in 1984 as an alternative to *local illumination models* such as Phong's model. See [17] and [29]. Their idea was to simulate the actual underlying physical phenomena using the radiosity equation that had been developed in the radiative heat transfer literature. The radiosity equation is given by

$$u(p) - \frac{\rho(p)}{\pi} \int_S V(p, q) G(p, q) u(q) dq = E(p), p \in S. \quad (1)$$

In this,  $S$  is contained in a closed environment in  $R^3$ , and it is often polyhedral.  $V(p, q)$  is the visibility function between two points  $p, q \in S$ , defined as

$$V(p, q) = \begin{cases} 1 & \text{if } \overleftrightarrow{pq} \cap S = \{p, q\}, \\ 0 & \text{otherwise.} \end{cases} \quad (2)$$

and  $G(p, q)$  is the radiosity kernel function defined as

$$G(p, q) = \frac{\cos(\theta_p) \cos(\theta_q)}{\|p - q\|^2},$$

where  $\theta_p$  and  $\theta_q$  are the angle between the line  $\overleftrightarrow{pq}$  and the normal vector  $n_p$  at  $p \in S$  and the normal vector  $n_q$  at  $q \in S$ , respectively. The direction  $n_q$  is the direction from which  $p$  is being viewed from  $q$ .

\* Corresponding author: e-mail: jseol@valdosta.edu, Phone: +01 229 259 2043, Fax: +01 229 219 1257

\*\* e-mail: atkinson@math.uiowa.edu, Phone: +01 319 335 0766, Fax: +01 319 335 0714

This equation is the result of applying the balance of energy to the radiosity under the assumption that all the surfaces are diffuse emitters, absorbers and reflectors in a nonparticipating medium, cf. [25]. Mathematically, it is a Fredholm integral equation of the second kind. In general, we use a numerical method to find an approximate solution of this equation. After solving (1) using various numerical methods, the value  $u(p)$  is used to determine the color values for the pixel  $p$  on the surface  $S$ . This rendering method is called a *global illumination model* since it takes the interreflection between all the surfaces into consideration.

One of the most popular numerical solution methods of solving (1) in computer graphics is the *piecewise constant Galerkin method*. Applying the piecewise constant Galerkin method to the radiosity equation, we obtain the following linear system.

$$B_i = E_i + \rho_i \sum_{j=1}^N F_{ij} B_j, \quad (3)$$

where

$$F_{ij} = \alpha_{ij} \int_{x \in P_i} \int_{y \in P_j} \frac{\cos(\theta_i) \cos(\theta_j)}{\pi r^2} V(x, y) dy dx. \quad (4)$$

Here,  $B_i$  is the radiosity that we want to find and  $F_{ij}$  is called the *form factor* between two elements  $P_i$  and  $P_j$ . Frequently equation (3) is called the radiosity equation in the computer graphics community instead of (1).

The linear system (3) is a dense matrix and there are  $n^2$  terms  $F_{ij}$ . Thus, it is important to find a fast and accurate method to evaluate  $F_{ij}$  in order to find a quality approximate solution of (3). Some of the special methods used to approximate the form factors are the ‘Monte Carlo method’, ‘crossed-strings method’, ‘unit sphere method’, and the ‘inside sphere method’. These methods have been developed in the radiative heat transfer community and adapted to computer graphics. In particular, the implementation of the unit sphere method using rendering hardware has been studied in [11]. It is also called the ‘hemi-cube method’.

In 1993, Peter Schröder presented a formula for  $F_{ij}$  between two general polygons. He derived the formula using repeated application of Stoke’s theorem. For more information, refer to [35]. More recently, Min Chen and James Arvo used the concept of generalized irradiance tensors to derive new closed-form expressions for computing the illumination from luminaires with linearly varying radiant exitance. The derivation of these expressions are based on the use of Clausen’s integral. For more details, refer to [7] and [8].

Another numerical method for solving (1) is the collocation method. General numerical methods for Fredholm integral equations of the second kind are given in [2]. Applying the piecewise constant collocation method to the radiosity equation, (1), we get the following linear system,

$$MB = E, \quad (5)$$

where

$$M_{ij} = \delta_{ij} - \frac{\rho(t_i)}{\pi} \int_{P_j} G(t_i, q) V(t_i, q) dS_q, \quad (6)$$

$$B_i = b_i, \quad (7)$$

$$E_i = E(t_i). \quad (8)$$

Again, the linear system (5) is a dense matrix with  $n^2$  double integrals to evaluate. In general, these integrals are nontrivial to evaluate, and they are the reason for this paper.

In the following section, we present an analysis of the numerical solution of the radiosity equation using the collocation method. We give general stability and convergence results for the collocation solution of the equation.

In §3 we show how to use affine transformation to convert the integration in  $M_{ij}$  into integrations over a standard integration domain  $\sigma$  that are easier to evaluate analytically. In §4 we introduce integrals  $H_{m,n,4}$ , and we show the analytic evaluation of  $H_{m,n,4}$  for  $m, n = 0, 1$  that is needed to solve (6). We also discuss possibilities and difficulties related to the analytic evaluation of  $H_{m,n,4}$  for other values of  $m$  and  $n$ . Experimental calculations of the analytic evaluation procedures are given in §5 for models that are commonly encountered in computer graphics.

## 2 Projection Methods for the Radiosity Equation

If we put the integral equation (1) into operator form, we have

$$(I - \mathcal{K})u = E. \tag{9}$$

In this,  $\mathcal{K}$  is an integral operator from a Banach space  $X$  to  $X$  defined as

$$\mathcal{K}u(p) = \frac{\rho(p)}{\pi} \int_S V(p, q)G(p, q)u(q) dq, \quad p \in S. \tag{10}$$

Usually,  $X = L^\infty(S)$  or  $L^2(S)$ . If the surface  $S$  is unoccluded, then we have  $V(p, q) = 1$  for all  $p, q \in S$  and the integral (10) simplifies into

$$\mathcal{K}u(p) = \frac{\rho(p)}{\pi} \int_S G(p, q)u(q) dq, \quad p \in S. \tag{11}$$

In order to solve (9) approximately, we choose a sequence of finite-dimensional subspaces  $X_n \subset X$  with  $\dim(X_n) = d_n < \infty$  and we try to find a function  $\bar{u}_n \in X_n$  such that the residual defined by

$$r_n = E - (I - \mathcal{K})\bar{u}_n \tag{12}$$

is made small in some sense. *Projection methods* use projection operators  $P_n : X \rightarrow X_n$  as a means to minimize the residual (12). For a given projection operator  $P_n : X \rightarrow X_n$ , our goal is to find  $\bar{u}_n \in X_n$  such that

$$P_n r_n = P_n[E - (I - \mathcal{K})\bar{u}_n] = 0. \tag{13}$$

Different projection operators lead to different approximate solution methods, cf. [2]. In the following sections we introduce *collocation methods*, one of the most popular projection methods. After that, we develop an evaluation method for integrals that are related to collocation methods since collocation methods are the main subject of this work.

### 2.1 Collocation Methods

We review the theoretical framework for collocation methods, emphasizing those aspects we need here. Let  $X_n = \text{span}\{l_j \in X \mid j = 1, 2, \dots, d_n\}$  be a subspace of  $X$  and let  $t_1, t_2, \dots, t_{d_n} \in S$  be fixed distinct points. Given  $u \in X$ , define  $P_n u$  to be the element of  $X_n$  that interpolates  $u$  at the nodes  $\{t_1, t_2, \dots, t_{d_n}\}$ . Thus, we can write

$$P_n u(t) = \sum_{j=1}^{d_n} b_j l_j(t), \tag{14}$$

with the coefficients  $\{b_j \mid j = 1, 2, \dots, d\}$  determined by solving the linear system

$$\sum_{j=1}^{d_n} b_j l_j(t_i) = u(t_i), \quad i = 1, 2, \dots, d_n.$$

This linear system has a unique solution if

$$\det[l_j(t_i)] \neq 0.$$

The projection operator  $P_n$  defined in (14) is called an *interpolatory projection operator*. Finding  $\bar{u}_n \in X_n$  that satisfies (13) is called a *collocation method* for obtaining an approximate solution of (9), cf. [2].

For instance, suppose  $S$  is a polyhedral surface composed of planar polygons  $\{S_j \subset R^3 \mid j = 1, \dots, N\}$  in  $R^3$ . We have

$$S = S_1 \cup S_2 \cup \dots \cup S_N. \tag{15}$$

We assume that  $S_j \cap S_k$  is (1) a line segment of the boundaries of  $S_j$  and  $S_k$ , (2) a vertex of  $S_j$  and  $S_k$ , or (3)  $S_j \cap S_k = \emptyset$ .

Let

$$T_n = \{\Delta_{n,k} \mid k = 1, 2, \dots, d_n\} \quad (16)$$

be a triangulation of  $S$  satisfying  $S = \cup_{k=1}^{d_n} \Delta_{n,k}$ , and for each  $k$ ,  $\Delta_{n,k} \subset S_i$  for some  $i = 1, 2, \dots, N$ . Let  $l_j$  be the characteristic function with support  $\Delta_{n,j}$ . Take  $X_n = \text{span}\{l_j \mid j = 1, 2, \dots, d_n\}$ . For fixed distinct points  $t_1, t_2, \dots, t_{d_n} \in S$  satisfying  $t_j \in \text{interior}(\Delta_{n,j})$ , we define a projection operator  $P_n : X \rightarrow X_n$  by

$$P_n u(t) = \sum_{j=1}^{d_n} u(t_j) l_j(t)$$

Note that

$$P_n u(t_i) = u(t_i), \text{ for } i = 1, 2, \dots, d_n, \quad (17)$$

and

$$l_j(t_i) = \delta_{ij}, \text{ for } i = 1, 2, \dots, d_n,$$

by the definition of  $P_n$  and  $l_j$ . Using this definition of  $P_n$  leads to the piecewise constant collocation method.

By using the collocation method to solve (9) approximately, we have

$$\begin{aligned} P_n[E - (I - \mathcal{K})\bar{u}_n] &= 0, \\ P_n[(I - \mathcal{K})\bar{u}_n] &= P_n(E), \\ (I - \mathcal{K})\bar{u}_n(t_i) &= E(t_i), \end{aligned} \quad (18)$$

for all  $i = 1, 2, \dots, d_n$ , by (17). Since  $\bar{u}_n \in X_n = \text{span}\{l_j \mid j = 1, 2, \dots, d_n\}$ , we have

$$\bar{u}_n = \sum_{j=1}^{d_n} b_j l_j. \quad (19)$$

Combining (18) and (19), we get

$$\begin{aligned} \bar{u}_n(t_i) - \mathcal{K}\bar{u}_n(t_i) &= E(t_i) \\ \sum_{j=1}^{d_n} b_j (l_j(t_i) - \frac{\rho(t_i)}{\pi} \int_{\Delta_{n,j}} V(t_i, q) G(t_i, q) l_j(q) dS_q) &= E(t_i) \end{aligned} \quad (20)$$

for  $i = 1, 2, \dots, d_n$ . Since

$$l_j(q) = \begin{cases} 1, & \text{if } q \in \Delta_{n,j}, \\ 0, & \text{otherwise,} \end{cases}$$

we have the following system of equations

$$\sum_{j=1}^{d_n} b_j (\delta_{ij} - \frac{\rho(t_i)}{\pi} \int_{\Delta_{n,j}} V(t_i, q) G(t_i, q) dS_q) = E(t_i), \quad (21)$$

for  $i = 1, 2, \dots, d_n$ , from equation (20).

In matrix form, (21) can be written as

$$MB = E,$$

with

$$M_{ij} = \delta_{ij} - \frac{\rho(t_i)}{\pi} \int_{\Delta_{n,j}} V(t_i, q)G(t_i, q)dS_q, \tag{22}$$

$$B_i = b_i, \tag{23}$$

$$E_i = E(t_i), \tag{24}$$

for  $i, j = 1, 2, \dots, d_n$ . By solving this linear system for  $B$ , we can get the approximate solution  $\bar{u}_n(t) = \sum_{j=1}^{d_n} b_j l_j(t) \in X_n$  of (9). When  $t_j$  is the centroid of  $\Delta_j$ , we refer to this collocation method as the *centroid method* for obtaining the approximate solution of (9).

We can use higher degree piecewise polynomial functions over the triangulation  $\{\Delta_{n,k} \mid k = 1, 2, \dots, d_n\}$  of  $S$  instead of using piecewise constant functions. In that case, we have to choose different node points depending on the degree of piecewise polynomial functions being used. See [2, Section 5.2] for a general schema for such methods.

When we consider an interpolatory projection operator in  $X = L^\infty(S)$ , the evaluation of  $u \in X$  at a point  $p \in S$  is not well-defined. This issue and other relevant considerations of the collocation method in  $L^\infty(S)$  have been considered and dealt with by Atkinson, Graham and Sloan in [4].

### 2.2 General Framework of the Projection Method

In this section we provide the analysis of the projection method for solving the radiosity equation. If we put the projection method for solving the radiosity equation in abstract framework, it can be written as

$$(I - P_n \mathcal{K})u_n = P_n E.$$

In here,  $P_n$  is an interpolatory projection operator on a Banach space  $X$ . We usually take  $X = L^\infty(S)$ .

In order to prove

$$\|\mathcal{K}\| < 1,$$

we use the following result, proven in [3].

**Lemma 2.1** Assume  $S$  is a polyhedral surface and  $p \in S^\circ$ , the interior of a face of  $S$ . Then, we have

$$\int_S V(p, q)G(p, q)dq \leq \pi. \tag{25}$$

The inequality (25) holds at all points  $p \in S$  for which  $S$  is smooth in some neighborhood of  $p$ . Since we have

$$\text{measure}\{p \in S \mid p \text{ does not have a smooth neighborhood in } S\} = 0,$$

we can say the inequality (25) is true almost everywhere. With this lemma, we can obtain that

$$\frac{\rho(p)}{\pi} \int_S V(p, q)G(p, q)dq \leq \rho(p) \leq \|\rho\|_\infty,$$

almost everywhere for  $p \in S$ . From this, we have

$$\|\mathcal{K}u\|_\infty = \left\| \frac{\rho(p)}{\pi} \int_S V(p, q)G(p, q)u(q)dq \right\|_\infty \tag{26}$$

$$\leq \|\rho\|_\infty \|u\|_\infty. \tag{27}$$

This means

$$\|\mathcal{K}\| \leq \|\rho\|_\infty.$$

Thus,  $\|\rho\|_\infty < 1$  implies that  $(I - \mathcal{K})^{-1}$  exists as a bounded linear operator from  $L^\infty(S)$  to  $L^\infty(S)$  and

$$\|(I - \mathcal{K})^{-1}\| \leq \frac{1}{1 - \|\mathcal{K}\|},$$

by the use of the geometric series theorem.

If we assume

$$\|P_n \mathcal{K}\| \leq \alpha < 1, \quad n \geq 1 \quad (28)$$

then it follows trivially that  $(I - P_n \mathcal{K})^{-1}$  exists and is uniformly bounded for  $n \geq 1$ , with

$$\|(I - P_n \mathcal{K})^{-1}\| \leq \frac{1}{1 - \alpha}, \quad n \geq 1 \quad (29)$$

With the centroid method, we have  $\|P_n\| = 1$ , and therefore

$$\|P_n \mathcal{K}\| \leq \|\mathcal{K}\| \leq \|\rho\|_\infty < 1$$

For higher degree interpolation, we would need to have

$$\alpha \equiv \left[ \sup_{n \geq 1} \|P_n\| \right] \|\rho\|_\infty < 1$$

in order to have (28) be satisfied. A less restrictive analysis is given in Hansen [21] to obtain (29).

Using the identity

$$(I - P_n \mathcal{K})(u - u_n) = u - P_n u$$

and assuming (28), we also have the following bounds

$$\frac{\|u - P_n u\|_\infty}{1 + \alpha} \leq \|u - u_n\|_\infty \leq \frac{\|u - P_n u\|_\infty}{1 - \alpha}, \quad n \geq 1$$

Therefore, the speed of convergence of  $u_n$  to  $u$  is the same as the speed of convergence of  $P_n u$  to  $u$  in  $X = L^\infty(S)$ . The latter is not true for many choices of  $u \in X$ ; but if  $u \in C(S)$ , then  $P_n u$  converges to  $u$  in  $X$ .

### 3 Calculation of the Collocation Integrals

If we assume that  $S$  is an unoccluded surface in  $R^3$ , the visibility function  $V(t_i, q) = 1$ . Thus, in order to solve the linear system (21) for unoccluded surface  $S$ , we are required to evaluate the following integral

$$\int_{\Delta_{n,j}} G(t_i, q) dS_q, \quad (30)$$

where  $\Delta_{n,j}$  is an arbitrary triangle in  $R^3$ . For this we convert the integral (30) into a sum of following form of integrals

$$\int_{\sigma} f(t_i, q) dS_q,$$

over the triangle  $\sigma = \{ (s, t, 0) \mid 0 \leq s \leq a, \text{ and } 0 \leq t \leq \frac{b}{a}s \}$ . We call this type of triangle a *standard integral domain*. In this section, we show how to use affine transformations to transform the integral (30) over a triangle  $\Delta$  in  $R^3$  into one or more integrals over a standard integral domain  $\sigma$ .

### 3.1 Affine Transformation from $R^3$ into $R^2$

We first show how to use an affine transformation to convert an integral over a triangle in  $R^3$  into an integral over a triangle in  $R^2$ .

**Definition 3.1** Let  $S$  be a  $n$ -polygon in  $R^3$  defined by the vertices  $v_0, v_1, \dots, v_{n-1}$  with  $v_0$  satisfying

$$\|v_0\| = \min\{\|v_i\| \mid i = 0, 1, \dots, n - 1\}$$

For  $S$  having the normal vector  $n_S$  which is equal to  $(1, \theta, \phi)$  in spherical coordinates, or  $(n_x, n_y, n_z)^T = (\sin(\phi) \cos(\theta), \sin(\phi) \sin(\theta), \cos(\phi))^T$  in rectangular coordinates, we define affine transformations  $A_S, B_S : R^3 \rightarrow R^3$  by

$$A_S q = U(q - v_0), \quad q \in R^3, \tag{31}$$

and

$$B_S r = v_0 + U^T r, \quad r \in R^3, \tag{32}$$

where  $U$  is a unitary transformation defined by

$$U = \begin{pmatrix} \cos(\theta) \cos(\phi) & \cos(\phi) \sin(\theta) & -\sin(\phi) \\ -\sin(\theta) & \cos(\theta) & 0 \\ \cos(\theta) \sin(\phi) & \sin(\theta) \sin(\phi) & \cos(\phi) \end{pmatrix}.$$

Note that  $U n_S = (0, 0, 1)^T$ . It is because the unitary transformation  $U$  rotates  $n_S$  with respect to  $z$ -axis by  $-\theta$  degrees first, and then it rotates the vector with respect to  $y$ -axis by  $\phi$  degrees. Since  $U$  is a unitary matrix, it is clear that

$$A_S B_S = B_S A_S = I_{R^3}. \tag{33}$$

By construction,  $A_S(S) \subset \{(s, t, 0) \mid s, t \in R\} \subset R^2$ . That is, the affine transformation  $A_S$  puts the  $n$ -polygon  $S$  into the  $xy$ -plane with the property that  $A_S(v_0) = 0$ .

Given  $p \in R^3$ , the normal  $n_p$  at  $p$ , and the  $n$ -polygon  $S \subset R^3$ , we consider the following integration:

$$\mathcal{K}u(p) = \int_S \frac{\langle p - q, n_q \rangle \langle q - p, n_p \rangle}{\|p - q\|^4} u(q) dS_q. \tag{34}$$

If we use the change of variable  $q = B_S r$  and (33), then (34) becomes

$$\mathcal{K}u(p) = \int_{A_S(S)} \frac{\langle p - B_S r, B_S(0, 0, 1) \rangle \langle B_S r - p, n_p \rangle}{\|A_S p - r\|^4} u(B_S r) dS_r. \tag{35}$$

$$= \langle p - B_S r, B_S(0, 0, 1) \rangle I_1 - \langle p - B_S r, B_S(0, 0, 1) \rangle I_2, \tag{36}$$

with

$$I_1 := \int_{A_S(S)} \frac{\langle B_S r, n_p \rangle}{\|A_S p - r\|^4} u(B_S r) dS_r \tag{37}$$

$$I_2 := \int_{A_S(S)} \frac{\langle p, n_p \rangle}{\|A_S p - r\|^4} u(B_S r) dS_r. \tag{38}$$

This uses the result that  $\langle p - B_S r, B_S(0, 0, 1) \rangle = \langle p - q, n_q \rangle$  is constant as  $q$  varies over  $S$ . It suffices to consider the integration  $I_1$  and  $I_2$  for a triangular region  $S$  in  $R^3$ , since an arbitrary  $n$ -polygon  $S$  can always be divided into triangles.

### 3.2 Affine Transformation into a Standard Integral Domain

The affine transformation  $A_S$  maps triangles in  $R^3$  into triangles in  $R^2$ . Now, we use the affine transformation defined in the following to transform a triangle in  $R^2$  into triangles that are standard integral domains.

**Definition 3.2** Let  $S$  be a triangle in  $R^2$  labelled by the vertices  $v_0 = 0, v_1, v_2$  counterclockwise, and let  $\psi \in [0, 2\pi)$  be the angle between the  $x$ -axis and vertex  $v_1$ . Then we can define the rotation,  $R_S : R^2 \rightarrow R^2$ , by

$$p \mapsto R_S p, \quad p \in R^2,$$

$$R_S = \begin{pmatrix} \cos(\psi) & \sin(\psi) & 0 \\ -\sin(\psi) & \cos(\psi) & 0 \\ 0 & 0 & 1 \end{pmatrix}.$$

By definition, the vertex  $R_S(v_0) = 0$  and the vertex  $R_S(v_1)$  is on the positive  $x$ -axis.

Using the rotations  $R_S$  and  $B_S$ , the integration  $I_1$  becomes

$$I_1 = \langle v_0, n_p \rangle \int_{R_{A_s(S)} A_S(S)} \frac{1}{\|R_{A_s(S)} A_S p - s\|^4} u(B_S R_{A_s(S)}^{-1} s) dS_s$$

$$+ \int_{R_{A_s(S)} A_S(S)} \frac{\langle U^T R_{A_s(S)}^{-1} s, n_p \rangle}{\|R_{A_s(S)} A_S p - s\|^4} u(B_S R_{A_s(S)}^{-1} s) dS_s. \quad (39)$$

In this, the vertex  $v_0$  is the vertex described in (31) and (32). Similarly, the integration  $I_2$  becomes

$$I_2 = \langle p, n_p \rangle \int_{R_{A_s(S)} A_S(S)} \frac{1}{\|R_{A_s(S)} A_S p - s\|^4} u(B_S R_{A_s(S)}^{-1} s) dS_s. \quad (40)$$

By combining (39) with (40), we get

$$\mathcal{K}u(p) = c_1 I_3 + c_2 I_4, \quad (41)$$

with

$$I_3 := \int_{R_{A_s(S)} A_S(S)} \frac{1}{\|R_{A_s(S)} A_S p - s\|^4} u(B_S R_{A_s(S)}^{-1} s) dS_s \quad (42)$$

$$I_4 := \int_{R_{A_s(S)} A_S(S)} \frac{\langle U^T R_{A_s(S)}^{-1} s, n_p \rangle}{\|R_{A_s(S)} A_S p - s\|^4} u(B_S R_{A_s(S)}^{-1} s) dS_s. \quad (43)$$

In here,  $c_1 = \langle p - B_S r, B_S(0, 0, 1) \rangle \langle v_0 - p, n_p \rangle$  and  $c_2 = \langle p - B_S r, B_S(0, 0, 1) \rangle$ .

In order to evaluate integrals  $I_3$  and  $I_4$  for various types of triangles in  $R^2$ , we classify  $R_{A_s(S)} A_S(S)$  according to the relative position of its vertices. Suppose  $R_{A_s(S)} A_S(S)$  is the triangle with vertices  $v_0 = (0, 0)$ ,  $v_1 = (x_1, 0)$ , and  $v_2 = (x_2, y_2)$ . Then the type of the triangle  $R_{A_s(S)} A_S(S)$  is determined by  $x_2$ . If  $0 < x_2 < x_1$ , then the triangle is a triangle of type *A*. If  $x_2 \leq 0$ , then the triangle is a triangle of type *B*. If  $x_2 > x_1$ , then the triangle is a triangle of type *C*. If  $x_2 = x_1$ , then the triangle is a triangle of type *D*. Note that any triangle of type *D* is a standard integral domain. We show that the triangles of type *A*, type *B*, and type *C* can be split and transformed affinely into two triangles of type *D*.

First, let's consider the evaluation of the integration  $I_3$  for various types of triangles.

**Type A triangle for  $I_3$ .** If the triangle  $R_{A_s(S)} A_S(S)$  is the triangle of type *A*, it can be split into two subtriangles  $T_1$  and  $T_2$  as shown in Figure 1. Then, we have

$$I_3 = \int_{T_1} \frac{1}{\|R_{A_s(S)} A_S p - s\|^4} u(B_S R_{A_s(S)}^{-1} s) dS_s \quad (44)$$

$$+ \int_{T_2} \frac{1}{\|R_{A_s(S)} A_S p - s\|^4} u(B_S R_{A_s(S)}^{-1} s) dS_s. \quad (45)$$

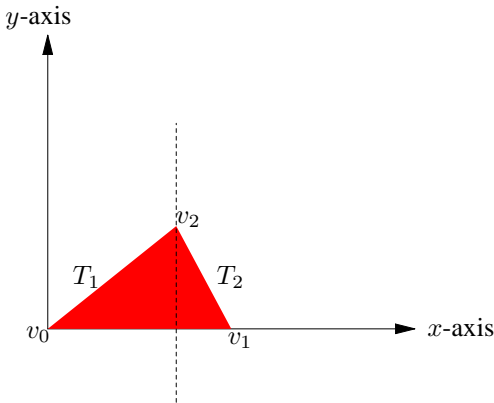


Fig. 1 Two subtriangles  $T_1$  and  $T_2$  of triangle type A

Note that triangle  $T_1$  in (44) is already a triangle of type  $D$ . In order to transform the triangle  $T_2$  into a triangle of type  $D$ , we use the following affine transformation.

**Definition 3.3** For a triangle  $T$  in  $R^2$  with vertices  $v_0 = 0, v_1,$  and  $v_2,$  we define  $M_{i,T} : R^2 \rightarrow R^2$  by

$$s \mapsto M_{i,T}(s), \text{ for } s \in R^2,$$

$$M_{i,T}(s) = R_{T-v_i}(s - v_i), \tag{46}$$

where the triangle  $T - v_i$  is the triangle  $T$  translated by  $-v_i$ .

For example, the affine transform  $M_{2,T_2}(T_2)$  of  $T_2$  is given by

$$M_{2,T_2}s = \begin{pmatrix} 0 & -1 & 0 \\ 1 & 0 & 0 \\ 0 & 0 & 1 \end{pmatrix} (s - v_2),$$

in matrix form since  $\psi = \frac{2\pi}{3}$  if  $R_{A_s(S)}A_S(S)$  is a triangle of type  $A$ .

Using the change of variable  $s = M_{2,T_2}^{-1}(t)$ , the integration in (45) becomes

$$\int_{M_{2,T_2}(T_2)} \frac{1}{\|M_{2,T_2}R_{A_s(S)}A_S p - t\|^4} u(B_S R_{A_s(S)}^{-1} M_{2,T_2}^{-1} t) dS_t.$$

It is clear that the triangle  $M_{2,T_2}(T_2)$  is of type  $D$ .

**Type B triangle for  $I_3$ .** If the domain  $D$  is the triangle  $R_{A_s(S)}A_S(S)$  of type  $B$ , we first affine transform the triangle into a triangle of type  $A$  using  $M_{1,D}$ . Since  $M_{1,D}(D)$  is a triangle of type  $A$ , we have

$$I_3 = \int_{M_{1,D}(D)} \frac{1}{\|M_{1,D}R_{A_s(S)}A_S p - (t)\|^4} u(B_S R_{A_s(S)}^{-1} M_{1,D}^{-1}(t)) dS_s. \tag{47}$$

using the change of variable  $t = M_{1,D}(s)$ . Once we have the integration(47) over  $M_{1,D}(D)$ , a triangle of type  $A$ , we can follow the same algorithm that is described in the above to handle the triangle of type  $A$ .

**Type C triangle for  $I_3$ .** Similarly, if the domain  $D$  is the triangle  $R_{A_s(S)}A_S(S)$  of type  $C$ , we first affine transform the triangle into a triangle of type  $A$  using  $M_{2,D}$ . Since  $M_{2,D}(D)$  is a triangle of type  $A$ , we have

$$I_3 = \int_{M_{2,D}(D)} \frac{1}{\|M_{2,D}R_{A_s(S)}A_S p - t\|^4} u(B_S R_{A_s(S)}^{-1} M_{2,D}^{-1}(t)) dS_t. \tag{48}$$

using the change of variable  $t = M_{2,D}(s)$ . Once we have the integration(48) over  $M_{2,D}(D)$ , a triangle of type  $A$ , we can follow the same algorithm that is described in the above to handle the triangle of type  $A$ .

The evaluation of the integration  $I_4$  for various domains types can also be handled in the similar way. For details, see [38].

#### 4 Analytic Evaluation of $H_{m,n,p}$

In this section, we study an analytic evaluation of the integrations that are needed for the setup of collocation methods for the radiosity equation.

**Definition 4.1** For  $m, n, p \geq 0$ , we define a function

$$H_{m,n,p} : R^3 \rightarrow R$$

by

$$H_{m,n,p}(x, y, z) = \int \int_{\Delta} \frac{\xi^m \eta^n}{((x - \xi)^2 + (y - \eta)^2 + z^2)^{p/2}} d\sigma(\xi, \eta). \quad (49)$$

In this, the region  $\Delta$  is a triangular region bounded by  $\xi = a, \eta = 0$ , and  $\eta = \frac{b}{a}\xi$ .

The analytic evaluation of this function when  $p$  is an odd integer is given in [22]. In this section, we consider the analytic evaluation of  $H_{m,n,4}(x, y, z)$  given in (49) for various  $m$  and  $n$  since these integers are the cases we need in order to evaluate exactly the integrals needed in implementing piecewise polynomial collocation methods. For piecewise polynomial collocation of degree  $r \geq 0$ , we need to evaluate  $H_{m,n,4}(x, y, z)$  for  $m, n \leq r + 1$ . If  $p = 4$ , then we will use the notation  $H_{m,n}$  instead of  $H_{m,n,4}$ .

In most cases, we are interested in evaluating the integration  $H_{m,n}(x, y, z)$  for  $z \neq 0$ , but we allow the use of very small  $z > 0$ . If the value of  $z$  is large enough, then the integrand (50)

$$k(x, y, z, \xi, \eta) = \frac{\xi^m \eta^n}{((x - \xi)^2 + (y - \eta)^2 + z^2)^2} \quad (50)$$

is well-behaved and the integral (49) is not hard to evaluate numerically. However, if the value of  $z$  is very small, then the denominator of the integrand (50) can be very small depending on the location  $x$  and  $y$ . In this case, the integrand  $k(x, y, z, \xi, \eta)$  behaves like it has a singularity at  $(\xi, \eta) = (x, y)$  making it difficult to evaluate numerically. For instance, if  $m = 0$  and  $n = 0$ , then

$$k(\xi, \eta, z, \xi, \eta) = \frac{1}{z^4}.$$

and a slight change in  $z$  makes a dramatic difference in the value of  $k(x, y, z, \xi, \eta)$  for  $(\xi, \eta)$  near  $(x, y)$ .

##### 4.1 Analytic Evaluation of $H_{m,n}$ for $m, n = 0, 1$

First, we consider the evaluation of  $H_{0,0}(x, y, z)$ . By definition, we have

$$H_{0,0}(x, y, z) = \int_0^a \int_0^{\frac{b}{a}\xi} \frac{1}{((x - \xi)^2 + (y - \eta)^2 + z^2)^2} d\eta d\xi.$$

Then,

$$H_{0,0}(x, y, z) = \frac{1}{2} \int_0^a \frac{\frac{b}{a}\xi - y}{((x - \xi)^2 + z^2)((x - \xi)^2 + z^2 + (\frac{b}{a}\xi - y)^2)} d\xi \quad (51)$$

$$+ \frac{1}{2} \int_0^a \frac{y}{((x - \xi)^2 + z^2)((x - \xi)^2 + z^2 + y^2)} d\xi \quad (52)$$

$$+ \frac{1}{2} \int_0^a \frac{\arctan\left(\frac{\frac{b}{a}\xi - y}{\sqrt{((x - \xi)^2 + z^2)}}\right)}{((x - \xi)^2 + z^2)^{\frac{3}{2}}} d\xi \quad (53)$$

$$+ \frac{1}{2} \int_0^a \frac{\arctan\left(\frac{y}{\sqrt{((x - \xi)^2 + z^2)}}\right)}{((x - \xi)^2 + z^2)^{\frac{3}{2}}} d\xi. \quad (54)$$

The integrations in (51), (52), (53) and (54) can be evaluated analytically using symbolic calculators such as Mathematica or Maple. For further explanation of these, refer to [38].

Next, let's consider the analytic evaluation of  $H_{1,0}(x, y, z)$ . By definition, we have

$$H_{1,0}(x, y, z) = \int \int_{\Delta} \frac{\xi}{((x - \xi)^2 + (y - \eta)^2 + z^2)^2} d\sigma.$$

Then,

$$xH_{0,0}(x, y, z) - H_{1,0}(x, y, z) \tag{55}$$

$$= \int_0^a \int_0^{\frac{b}{a}\xi} \frac{(x - \xi)^1}{((x - \xi)^2 + (y - \eta)^2 + z^2)^2} d\eta d\xi. \tag{56}$$

Setting  $u = x - \xi$  and  $v = y - \eta$ , the integration (56) becomes

$$\int_x^{x-a} \frac{u \left(\frac{b}{a}(u - x) + y\right)}{2(u^2 + (\frac{b}{a}(u - x) + y)^2 + z^2)(u^2 + z^2)} du \tag{57}$$

$$- \int_x^{x-a} \frac{u y}{2(u^2 + y^2 + z^2)(u^2 + z^2)} du \tag{58}$$

$$+ \int_x^{x-a} \frac{u}{2(u^2 + z^2)^{\frac{3}{2}}} \arctan\left(\frac{b(u - x) + ay}{a\sqrt{u^2 + z^2}}\right) du \tag{59}$$

$$- \int_x^{x-a} \frac{u}{2(u^2 + z^2)^{\frac{3}{2}}} \arctan\left(\frac{y}{\sqrt{u^2 + z^2}}\right) du. \tag{60}$$

With the help of Mathematica, we can obtain the analytic evaluation of these integrals in (57), (58), (59) and (60). For further explanation of these, refer to [38]. Thus, we can analytically evaluate  $H_{1,0}(x, y, z)$  using (55) and (56).

We can evaluate  $H_{0,1}(x, y, z)$  in a similar manner to get

$$\begin{aligned} H_{0,1}(x, y, z) &= yH_{0,0}(x, y, z) - \frac{a}{2\sqrt{\alpha + a^2 z^2}} \arctan\left(\frac{ax + by}{\sqrt{\alpha + a^2 z^2}}\right) \\ &+ \frac{a}{2\sqrt{\alpha + a^2 z^2}} \arctan\left(\frac{ax + by - a^2 - b^2}{\sqrt{\alpha + a^2 z^2}}\right) \\ &+ \frac{1}{2\sqrt{y^2 + z^2}} \arctan\left(\frac{x}{\sqrt{y^2 + z^2}}\right) - \frac{1}{2\sqrt{y^2 + z^2}} \arctan\left(\frac{x - a}{\sqrt{y^2 + z^2}}\right). \end{aligned}$$

Finally, we consider the analytic evaluation of  $H_{1,1}(x, y, z)$ . For that, we use the following identity.

$$\int \int_{\Delta} \frac{(x - \xi)(y - \eta)}{((x - \xi)^2 + (y - \eta)^2 + z^2)^2} d\sigma \tag{61}$$

$$= xyH_{0,0} - xH_{0,1} - yH_{1,0} + H_{1,1}. \tag{62}$$

Since we know the analytic evaluations of  $H_{0,0}(x, y, z)$ ,  $H_{1,0}(x, y, z)$  and  $H_{0,1}(x, y, z)$ , it suffices to find the analytic evaluation of (61) to find the analytic evaluation of  $H_{1,1}(x, y, z)$ .

Using the same change of variable that has been used to find the analytic evaluation of (56), we can find the analytic evaluation of (61). Therefore, the analytic evaluation of  $H_{1,1}$  can be found by solving (61) and (62) for  $H_{1,1}$ .

#### 4.2 Analytic Evaluation of $H_{m,n}$ for general $m$ and $n$

For larger values of  $m, n$ , we use recursion to aid in evaluating  $H_{m,n}(x, y, z)$ . This will work for most but not all values of  $m, n$ , leading to formulas of the type given above. For certain special values of  $m, n$ , e.g.  $(m, n) = (2, 0)$ , we will need to use yet another technique. We begin our consideration of larger values of  $m, n$  with the following recursion formula; a proof is given in [38]

**Lemma 4.2** *Suppose  $\Delta$  is a right triangle and  $\nu$  the outward normal vector at a point on the boundary  $\partial\Delta$  of the triangle. Then, we have*

$$\int_{\partial\Delta} \frac{\xi^{m-1}\eta^n}{(x-\xi)^2 + (y-\eta)^2 + z^2} \cos(\nu, \xi) dl = (m-1)H_{m-2,n,2}(x, y, z) + 2xH_{m-1,n}(x, y, z) - 2H_{m,n}(x, y, z), \quad (63)$$

and

$$\int_{\partial\Delta} \frac{\xi^m\eta^{n-1}}{(x-\xi)^2 + (y-\eta)^2 + z^2} \cos(\nu, \eta) dl = (n-1)H_{m,n-2,2}(x, y, z) + 2yH_{m,n-1}(x, y, z) - 2H_{m,n}(x, y, z). \quad (64)$$

In here,  $\cos(\nu, \xi)$  is the cosine angle between the vector  $\nu$  and  $\xi - x$  axis. Similarly,  $\cos(\nu, \eta)$  is the cosine angle between the vector  $\nu$  and  $\eta - y$  axis

In general, the analytic evaluation of  $H_{m,n}(x, y, z)$  for  $m \geq 2$  or  $n \geq 2$  can be simplified by using the above lemma. As long as we can find the analytic evaluations of integrals (63), (64),  $H_{m,n-2,2}$  and  $H_{m-2,n,2}$ , we can find the analytic evaluation of  $H_{m,n}(x, y, z)$ . It is relatively easy to evaluate (63) and (64) analytically since they are line integrals. The main difficulty comes from evaluating  $H_{m,n-2,2}$  and  $H_{m-2,n,2}$ .

As an example of Lemma 4.2, we discuss an evaluation method for  $H_{2,0}(x, y, z)$ . By use of (63), we have

$$H_{2,0}(x, y, z) = \frac{1}{2} H_{0,0,2}(x, y, z) + xH_{1,0}(x, y, z) - \frac{1}{2} \int_{\partial\Delta} \frac{\xi^1}{(x-\xi)^2 + (y-\eta)^2 + z^2} \nu_\xi dl. \quad (65)$$

Thus, we can evaluate  $H_{2,0}(x, y, z)$  analytically if we can find an analytic evaluation of  $H_{0,0,2}(x, y, z)$  and the line integral in (65)

The analytic evaluation of (65) can be simplified by using the assumption that the integration domain  $\partial\Delta$  is the boundary of a right triangle. Thanks to this assumption, we have that  $\nu_\xi = 1$  on  $e_v$  and  $\nu_\xi = 0$  on  $e_h$ . That is, the integral in (65) becomes

$$\nu_\xi \int_{e_d} \frac{\xi}{(x-\xi)^2 + (y-\eta)^2 + z^2} dl \quad (66)$$

$$+ \int_{e_v} \frac{\xi}{(x-\xi)^2 + (y-\eta)^2 + z^2} dl. \quad (67)$$

where  $e_h$ ,  $e_v$ , and  $e_d$  are horizontal, vertical, and diagonal edge of the triangle  $\Delta$ , respectively. The integrations in (66) and (67) can be evaluated analytically.

Next, we discuss the analytic evaluation of  $H_{0,0,2}$ . By definition, we have

$$H_{0,0,2}(x, y, z) = \int \int_{\Delta} \frac{1}{(x-\xi)^2 + (y-\eta)^2 + z^2} d\sigma(\xi, \eta) \quad (68)$$

$$= \int \int_{\Sigma} \frac{1}{u^2 + v^2 + z^2} d\sigma(u, v) \quad (69)$$

for  $u = \xi - x$  and  $v = \eta - y$ . The integration domain  $\Sigma$  is shown in Figure 2 that we can get after translating the original integration domain  $\Delta$  by  $(x, y)$ . Since there is no rotation involved,  $\Sigma$  always has the vertical and

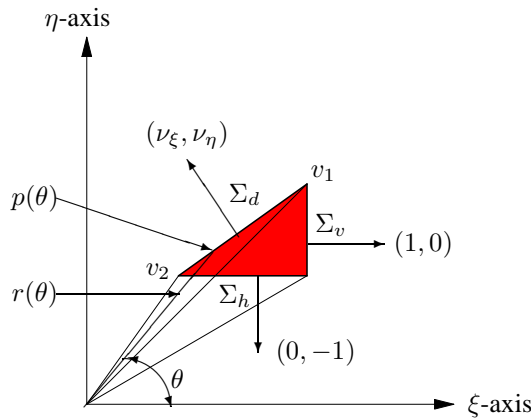


Fig. 2 Splitting integral domain  $\Sigma$  into subtriangles

horizontal edges. In order to evaluate this integration analytically, we split the integration (69) into three parts as shown in Figure 2.

$$H_{0,0,2}(x, y, z) = \text{sign}(\Sigma_d) \int \int_{\Sigma_d} \frac{1}{u^2 + v^2 + z^2} d\sigma(u, v) \tag{70}$$

$$+ \text{sign}(\Sigma_h) \int \int_{\Sigma_h} \frac{1}{u^2 + v^2 + z^2} d\sigma(u, v) \tag{71}$$

$$+ \text{sign}(\Sigma_v) \int \int_{\Sigma_v} \frac{1}{u^2 + v^2 + z^2} d\sigma(u, v) \tag{72}$$

In this,  $\Sigma_d$  is the triangle formed by connecting  $(0, 0)$  and the two vertices of the hypotenuse of the right triangle  $\Sigma$ . The triangles  $\Sigma_v$  and  $\Sigma_h$  are formed similarly by connecting  $(0, 0)$  and the vertical and horizontal edges of the triangle  $\Sigma$  respectively. The values of  $\text{sign}(\Sigma_h)$ ,  $\text{sign}(\Sigma_v)$ , and  $\text{sign}(\Sigma_d)$  take on either  $-1, 0$  or  $1$ . They are determined so as to hold the equality in (70). For specific determination of these values, refer to the table given on page 106 in [38].

We first consider the integration over  $\Sigma_d$  in order to evaluate  $H_{0,0,2}(x, y, z)$ . Let's suppose  $p(\theta)$  is a point on the hypotenuse whose angle is  $\theta$  with respect to  $x$  axes and  $v_1 = (x_1, y_1)$  and  $v_2 = (x_2, y_2)$  are the two vertices of the hypotenuse of the right triangle  $\Sigma$ . The angle  $\theta_1$ , and  $\theta_2$  are the angles that  $v_1$  and  $v_2$  make with respect to  $x$  axes respectively. Define  $r(\theta)$  to be the distance from the origin to  $p(\theta)$ . See Figure 2. Then, by setting  $u = r \cos(\theta)$  and  $v = r \sin(\theta)$ , we have

$$\int \int_{\Sigma_d} \frac{1}{u^2 + v^2 + z^2} d\sigma(u, v) = \frac{1}{2} \int_{\theta_1}^{\theta_2} \log(r(\theta)^2 + z^2) d\theta - \log(z)(\theta_2 - \theta_1). \tag{73}$$

In order to find the analytic evaluation of (73), it suffices to find the analytic evaluation of

$$\frac{1}{2} \int_{\theta_1}^{\theta_2} \log(r(\theta)^2 + z^2) d\theta. \tag{74}$$

First, we define  $s(\theta)$  as

$$s(\theta) = \frac{\|v_1 - p(\theta)\|}{\|v_1 - v_2\|}.$$

Then, we have

$$p(\theta) = (x_1 + s(\theta)(x_2 - x_1), y_1 + s(\theta)(y_2 - y_1)). \tag{75}$$

For all points  $p(\theta)$  on the hypotenuse, the value of  $s(\theta)$  is between 0 and 1. By (75), we have

$$\tan(\theta) = \frac{y_1 + s(\theta)(y_2 - y_1)}{x_1 + s(\theta)(x_2 - x_1)}, \quad (76)$$

$$\theta = \arctan\left(\frac{y_1 + s(\theta)(y_2 - y_1)}{x_1 + s(\theta)(x_2 - x_1)}\right), \quad (77)$$

$$d\theta = \frac{x_1 y_2 - x_2 y_1}{r(\theta)^2} ds. \quad (78)$$

We can also derive the following relation between  $r(\theta)$  and  $s(\theta)$ .

$$r(\theta)^2 = [(x_1 + s(\theta)(x_2 - x_1))^2 + (y_1 + s(\theta)(y_2 - y_1))^2] \quad (79)$$

By (78) and (79), the integration (74) becomes

$$\frac{(x_1 y_2 - x_2 y_1)}{2} \int_0^1 \frac{\log(\alpha s^2 + \beta s + \gamma)}{\alpha s^2 + \beta s + \gamma} ds \quad (80)$$

where

$$\begin{aligned} \alpha &= (x_2 - x_1)^2 + (y_2 - y_1)^2, \\ \beta &= 2(x_1(x_2 - x_1) + y_1(y_2 - y_1)), \\ \gamma &= x_1^2 + y_1^2 + z^2. \end{aligned}$$

The functional behavior of the integrand of (80) can be understood by considering the discriminant  $D$  and the minimum value of  $\alpha s^2 + \beta s + \gamma$  for  $s$ ,  $0 \leq s \leq 1$ . Let us consider the discriminant  $D$  given by

$$\frac{D}{4} = -(x_1 y_2 - y_1 x_2)^2 - \|v_1 - v_2\|^2 z^2.$$

Since  $\|v_1 - v_2\|^2 z^2 > 0$ , we have  $\frac{D}{4} < 0$ . Thus, we can say

$$\alpha s^2 + \beta s + \gamma > 0 \quad (81)$$

for all  $s \in [0, 1]$  because  $\alpha > 0$ ,  $\gamma > 0$ .

By setting  $v_1 = (r_1 \cos(\theta_1), r_1 \sin(\theta_1))$  and  $v_2 = (r_2 \cos(\theta_2), r_2 \sin(\theta_2))$  the minimum value of  $\alpha s^2 + \beta s + \gamma$  is given by

$$\frac{4\alpha\gamma - \beta^2}{4\alpha} = \frac{(r_1 r_2)^2 \sin^2(\theta_2 - \theta_1)}{\|v_1 - v_2\|^2} + z^2 \geq z^2 \quad (82)$$

This means the minimum of the quadratic equation  $\alpha s^2 + \beta s + \gamma$  becomes close to  $z^2$  as the difference between angles of the vertices  $v_1$  and  $v_2$  becomes small. Thus, we can say the integrand

$$\frac{\log(\alpha s^2 + \beta s + \gamma)}{\alpha s^2 + \beta s + \gamma} \quad (83)$$

in (80) is smooth by (81), but becomes increasingly ill-behaved as the aspect ratio of the triangle  $\Sigma_d$  becomes smaller since  $\frac{\log(x)}{x} \rightarrow -\infty$  as  $x$  approaches to 0. See Figure 3.

We can use a symbolic calculator such as Mathematica to evaluate the integral in (80) analytically. This is more difficult to use practically since it involves integration in the complex domain and the use of the dilogarithm function. See [38]. In complex geometries used in practical computer graphics, most triangulation schemes such as Delaunay triangulation avoid the use of triangles with low aspect ratio. Thus, it could be practically more desirable to use a numerical scheme to evaluate (80).

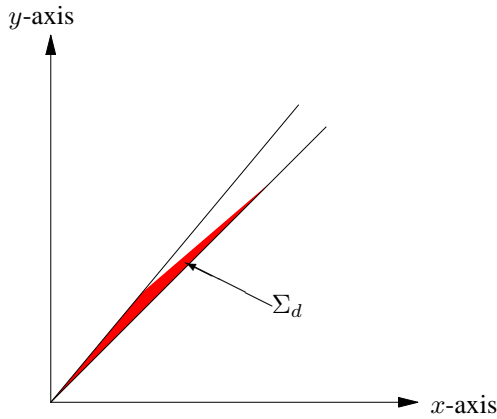


Fig. 3 Triangle  $\Sigma_d$  with low aspect ratio

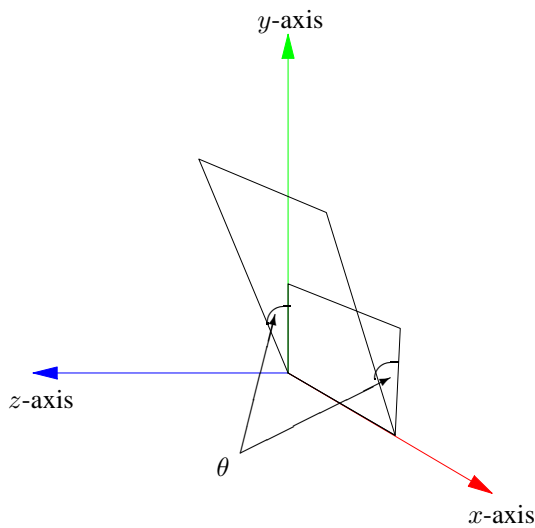


Fig. 4 Two planes joining with angle  $\theta$

### 5 Numerical Experiments for Sample Models

For our numerical experiments, we have chosen three different surface models. These models are the configuration that are most commonly encountered in computer graphics to make up bigger scene, cf. [19], [23], and [10]. Using these models and properly chosen test solutions, we have tested timing, accuracy, and the effect of different subdivision schemes. We first introduce the models.

- Model 1. This first model is made of two rectangles, denoted by  $S_1$  and  $S_2$  as illustrated in Figure 4. The dimensions of  $S_1$  and  $S_2$  are given by

$$S_1 = \{(x, y, 0) \mid 0 \leq x \leq 200, 0 \leq y \leq 100\},$$

$$S_2 = \left\{ \left( x, y, \frac{y}{2} \right) \mid 0 \leq x, y \leq 200 \right\}.$$

The surfaces  $S_1$  and  $S_2$  joins with each other along a common edge at an angle  $\theta = 26.5651^\circ$ . This angle is the result of choosing two rectangles  $S_1$  and  $S_2$  with integer vertex coordinates that are easier to render on the computer screen coordinate.

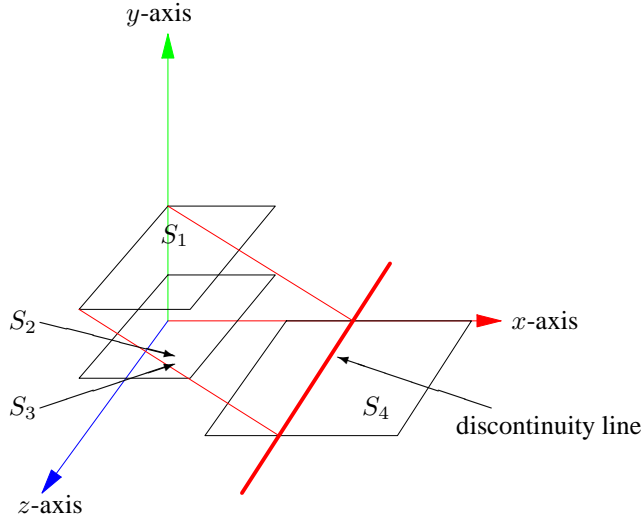


**Fig. 5** Four planes with discontinuity line.

- Model 2. This model is made of two perpendicular surfaces, denoted by  $S_1$  and  $S_2$ . This is like model 1, but with  $\theta = 90^\circ$ . The dimensions of  $S_1$  and  $S_2$  are given by

$$S_1 = \{(x, y, 0) \mid 0 \leq x \leq 200, 0 \leq y \leq 100\},$$

$$S_2 = \{(x, 0, z) \mid 0 \leq x, z \leq 200\}.$$

- Model 3. This model is made of four surfaces, denoted by  $S_1$ ,  $S_2$ ,  $S_3$ , and  $S_4$  as illustrated in Figure 5. The dimensions of  $S_1$ ,  $S_2$ ,  $S_3$ , and  $S_4$  are given by

$$S_1 = \{(x, 240, z) \mid 0 \leq x \leq 120, 0 \leq z \leq 280\},$$

$$S_2 = \{(x, 120, z) \mid 0 \leq x \leq 120, 0 \leq z \leq 280\},$$

$$S_3 = \{(x, 120, z) \mid 0 \leq x \leq 120, 0 \leq z \leq 280\},$$

$$S_4 = \{(x, 0, z) \mid 120 \leq x \leq 400, 0 \leq z \leq 280\}.$$

The dimensions of the models are chosen to be compatible with computer graphics applications. That is why we use relatively high values like 120, 200, and the angle  $\theta = 26.5651$ . These numbers are easy to render in computer graphics. Even if the surfaces  $S_2$  and  $S_3$  have the same dimension, we assume that the normal vector of  $S_2$  is  $(0, 1, 0)$ , directed upward, and the normal vector of  $S_3$  is  $(0, -1, 0)$ , directed downward.

We applied both the *analytic integration method* developed in the previous sections and a numerical integration scheme to evaluate

$$\int_{\Delta} \frac{\cos(\theta_p) \cos(\theta_q)}{\|p - q\|^2} dq. \quad (84)$$

This integration is needed to setup the matrix of the centroid collocation method. The numerical method that we used for comparison to the analytic evaluation method is based on converting the integral to a new integral of the form

$$\int_{\sigma} g(s, t) d\sigma,$$

over the unit simplex  $\sigma = \{(s, t) : 0 \leq s, t, s + t \leq 1\}$ .

Among a number of well-known numerical approximations to such integrals, we use a composite method that uses the following integration scheme:

$$\int_{\sigma} g(s, t) d\sigma \approx \sum_{j=1}^7 w_j g(\rho_j).$$

$n$	Analytic	7-point			
	$T_a$	$T_3$	$E_n$	$T_5$	$E_n$
4	0	0	$4.4138E - 4$	0.016	$6.8343E - 8$
16	0.031	0.016	$1.1786E - 4$	0.25	$3.5253E - 8$
64	0.532	0.22	$5.8931E - 5$	4.499	$1.7629E - 8$
256	34.73	4.416	$3.58934E - 5$	68.323	$8.74784E - 9$

**Table 1** Matrix setup error and timing comparison for model 1

$n$	Analytic	7-point			
	$T_a$	$T_3$	$E_n$	$T_5$	$E_n$
4	0	0	$4.9683E - 6$	0.016	$9.4203E - 10$
16	0	0.016	$3.8486E - 6$	0.281	$4.7163E - 10$
64	0.765	0.33	$1.9255E - 6$	4.155	$2.3612E - 10$
256	28.181	4.526	$8.7804E - 7$	69.324	$1.18182E - 10$

**Table 2** Matrix setup error and timing comparison for model 2

In this, the weights  $w_j$  and nodes  $\rho_j$  taken from the formula T2:5-1 of Stroud [42]. This numerical integration scheme has degree of precision 5. In order to improve the accuracy of this method, we use the 7-point method over  $4^\mu$  smaller triangles that we obtain by applying  $\mu$  levels of subdivisions to  $\Delta$ . We refer to this composite scheme as the *7-point method with  $\mu$  levels of subdivision*.

We present matrix setup timing in seconds and error comparisons for models 1 and 2 in Tables 2 and 1, respectively. The number  $n$  is the number of elements that we use for the test, and  $T_a$ ,  $T_3$ , and  $T_5$  are the times taken by the analytic integration method, the 7-point method with  $\mu = 3$  levels and the 7-point method with  $\mu = 5$  levels, respectively, to evaluate the integration (84). The error  $E_n$  is the averaged sum of all the differences of the analytic evaluation and numerical evaluation of the integration (84) at the node points. By studying Tables 2 and 1, we observe that the analytic method is faster than the 7-point method with level  $\mu = 5$ , but is more expensive than the 7-point method with level  $\mu = 3$ . Even if 7-point method with level  $\mu = 3$  is better than the analytic method in terms of speed, it shows a significant error when compared to the analytic evaluation method. The error becomes worse as the angle  $\theta$  between the two surfaces becomes smaller.

In these tests, it should be noted that the analytic method is implemented in C++ using STL template classes, whereas the 7-point method is implemented in Fortran. It is a generally well-known fact that the C++ implementation with STL templates is slower than a Fortran implementation. Considering this, the analytic method shows relatively good performance over the 7-point method. The timings were done on HP Compaq D530 CMT Desktop with a 3.0 GHz Pentium 4 CPU and 512 MB RAM running the Windows XP Professional operating system. The Fortran programs that we used are part of BIEPACK [1].

Next, we use models 2 and 3 with properly chosen true solutions  $u$  to test the accuracy of the approximate solution  $u_n$  obtained using the analytic method to solve the radiosity equation.

In order to test the collocation method, we choose a true function  $u(x, y, z)$  and we then calculate the emissivity  $E$  using highly accurate numerical integration. The collocation method is applied to find the approximate solution  $u_n$ , that is then compared to the known true solution  $u$ .

The true solution that we will use for model 2 is given by

$$u(x, y, z) = \begin{cases} 0 & \text{otherwise} \\ z^\beta & y = 0 \end{cases} \quad (85)$$

That is,  $u(x, y, z) = 0$  on  $S_2$  and  $u(x, y, z) = z^\beta$  on  $S_1$ . This test solution is chosen since it is proven in [32] that for most given emissivity functions  $E$ ,  $u$  has the behavior

$$u(x, 0, z) = g(z) + O(z^\beta), \quad z \rightarrow 0 \quad (86)$$

$n$	metric= $\ \cdot\ _1/n$		metric= $\ \cdot\ _\infty$	
	$E_n$	Ratio	$E_n$	Ratio
4	0.5178890		1.1241126	
16	0.2097839	2.4687	1.0240879	1.0976
64	0.0845805	2.4802	0.7981865	1.2830
256	0.0332735	2.5419	0.5772808	1.3827
1024	0.0125731	2.6464	0.4086213	1.4128

**Table 3** Centroid collocation errors of  $u$  with  $\beta = 0.5$  and uniform meshing on model 2

$n$	metric= $\ \cdot\ _1/n$		metric= $\ \cdot\ _\infty$	
	$E_n$	Ratio	$E_n$	Ratio
4	4.1403802		8.5621539	
16	1.3010115	3.1824	6.5596009	1.3052
64	0.4049425	3.2128	3.9413914	1.6642
256	0.1237672	3.2718	2.1854562	1.8038
1024	0.0366162	3.3801	1.1736712	1.8621

**Table 4** Centroid collocation errors of  $u$  with  $\beta = 0.9$  and uniform meshing on model 2

with a smooth function  $g(z)$  and  $\beta, 0 < \beta < 1$ , at the common edge. If the solution  $u$  satisfies (86), we can prove that

$$\|u - P_n u\|_\infty = O(h^\beta).$$

We use the solution (85) for model 2 with  $\beta = 0.5$  and  $0.9$  to test the effect of an algebraic singularity along the common edge.

The test results for  $\beta = 0.5$  are given in Table 3 for uniform meshing. In the case of uniform meshing, the expected rate of convergence is  $O(h^{0.5})$  as explained in the above. Table 3 shows that the rate of convergence is getting close to  $O(h^{0.5})$  as the number of elements  $n$  increases. The column labelled 'Ratio' denotes the ratio  $\frac{E_{n/4}}{E_n}$ . The test results for  $\beta = 0.9$  are given in Table 4 for uniform meshing. In the case of uniform meshing, the expected rate of convergence is  $O(h^{0.9})$ . The test results in Table 4 show that the rate of convergence is getting close to this theoretical expectation for  $\beta = 0.9$  as we increase the number of elements  $n$ .

The true solution that we use for model 3 is given by

$$u(x, y, z) = \begin{cases} 0 & \text{otherwise} \\ e^{-\gamma(x-d)}(x-d)^\beta & x > d \text{ and } y = 0 \end{cases}, \quad (87)$$

where  $d = 240$ . The line  $x = d$  on the  $xz$ -plane is the discontinuity line. To see the effect of a discontinuity in a derivative of  $u$  along this line, we solve the radiosity equation for  $u$  given by (87) with  $\beta = 0.5$  and  $\gamma = 0.02$ .

We present the numerical testing result for both uniform meshing and discontinuity meshing. Tables 5 and 6 shows the testing results for uniform meshing and discontinuity meshing, respectively. Table 5 reveals that the rate of convergence with uniform meshing is higher than the theoretical expectation of  $O(h^{1.5})$  as given in [3]. We expect the higher rate of convergence will settle down eventually as the number of elements increases. We can also observe that discontinuity meshing is no better than the uniform meshing as far as the rate of convergence is concerned. For additional explanation of discontinuity meshing and numerical examples, see [3] and [23].

**Acknowledgements** The work by the first author is supported in part by Valdosta State University faculty research grant.

$n$	metric= $\ \cdot\ _1/n$		metric= $\ \cdot\ _\infty$	
	$E_n$	Ratio	$E_n$	Ratio
8	0.0175512		0.0733565	
32	0.0404968	0.43340	0.0919982	0.79737
128	$2.9749E-3$	1.36131	$7.2977E-3$	1.26064
512	$1.9097E-4$	15.57758	$5.2234E-4$	13.97122
2048	$6.2298E-5$	3.06543	$1.9211E-4$	2.71896

**Table 5** Centroid collocation errors of  $u$  with  $(\beta, \gamma) = (0.5, 0.02)$  and uniform meshing on model 3

$n$	metric= $\ \cdot\ _1/n$		metric= $\ \cdot\ _\infty$	
	$E_n$	Ratio	$E_n$	Ratio
10	0.0024520		0.0080658	
40	0.0078304	0.31314	0.0212920	0.37882
160	$4.7525E-4$	1.64764	0.0132318	1.60915
640	$1.9943E-4$	2.38304	$6.0086E-4$	2.20214
2560	$7.3112E-5$	2.72773	$2.1996E-4$	2.73168

**Table 6** Centroid collocation errors of  $u$  with  $(\beta, \gamma) = (0.5, 0.02)$  and discontinuity meshing on model 3.

## References

- [1] Kendall E. Atkinson, *User's Guide to a Boundary Element Package for Solving Integral Equations on Piecewise Smooth Surfaces (Release #2)*, Reports on Computational Mathematics #102, Dept of Mathematics, University of Iowa, 1998.
- [2] Kendall E. Atkinson, *The Numerical Solution of Integral Equations of the Second Kind*, Cambridge University Press, 1997.
- [3] Kendall E. Atkinson, David Chien, Jaehoon Seol, *Numerical Analysis of the radiosity equation using the collocation method*, Electronic Transactions on Numerical Analysis 11 (2000), pp. 94-120.
- [4] Kendall E. Atkinson, I. Graham, and I. Sloan, *Piecewise Continuous Collocation in Integral Equations*, SIAM Journal of Numerical Analysis, 20:172-186, 1983.
- [5] Kendall E. Atkinson and Weimin Han, *Theoretical Numerical Analysis: A functional analysis framework*, Springer-Verlag, New York, 2001.
- [6] Mark de Berg et. al., *Computational Geometry: Algorithms and Applications*, Springer-Verlag, New York, 2000.
- [7] Min Chen and James Arvo, *A Closed-Form Solution for the Irradiance due to Linearly-Varying Luminaries*, Proceedings of the Eleventh Eurographics Workshop on Rendering, Pages 137-148.
- [8] Min Chen and James Arvo, *Simulating Non-Lambertian Phenomena Involving Linearly-Varying Luminaries*, Proceedings of the Twelfth Eurographics Workshop on Rendering, London, June 2001.
- [9] Per H. Christensen, Eric J. Stollnitz, Tony D. DeRose, David H. Salesin, *Wavelet Radiance*, Proceedings of the Fifth Eurographics on Rendering, Pages 287-302.
- [10] M. F. Cohen and J. R. Wallace, *Radiosity and Realistic Image Synthesis*, Academic Press Professional, 1993.
- [11] M. F. Cohen, and D. P. Greenberg, *The Hemi-Cube: A Radiosity Solution for Complex Environments*, Computer Graphics 19, 3 ( July 1985), 31-40.
- [12] Fredo Durand, George Drettakis and Claude Puech, *3D visibility made visibly simple: an introduction to the visibility skeleton*, Proceedings of the 24th annual conference on Computer graphics & interactive techniques, 1997, Pages 89 - 100.
- [13] J. D. Foley, et.al, *Computer Graphics : Principles and Practice in C*, Addison Wesley Longman, Inc., 1995.
- [14] A. Glassner, *An Introduction to Ray Tracing*, Academic Press, 1989.
- [15] Z. Gigus and J. Malik, *Computing the Aspect Graph for Line Drawings of Polyhedral Objects*, IEEE Trans. Pattern Analysis and Machine Intelligence, Vol. 1, No 2, Feb. 1990, pp 113-122.
- [16] Z. Gigus, J. Canny, and R. Seidel, *Efficiently Computing and Representing Aspect Graphs of Polyhedral Objects*, IEEE Trans. Pattern Analysis and Machine Intelligence, Vol. 13, No. 6, June 1991, pp 542-551.
- [17] C. M. Goral, K. E. Torrance, D. P. Greenberg, and B. Battaile, *Modelling the interaction of light between diffuse surfaces*, Computer Graphics(SIGGRAPH '84 Proceedings), vol.18, pp 212-222.
- [18] R. Hall, *Illumination and Color in Computer Generated Imagery*, Springer-Verlag, New York, 1989.
- [19] P. Hanrahan and D. Saltzman, *A Rapid Hierarchical Radiosity Algorithm for Unoccluded Environments*, Photorealism in Computer Graphics, Springer-Verlag, New York, Eurographics Seminar series, 1992.

- [20] O. Hansen, *The Radiosity Equation on Certain Spaces of Continuous Functions and its Numerical Solution*, Preprint 2, Habilitationsschrift, Fachbereichs Mathematik, der Johannes Gutenberg-Universität Mainz, 2001
- [21] O. Hansen, *On the stability of the collocation method for the radiosity equation on polyhedral domains*, IMA J. Numer. Anal. 22 (2002), pp. 463-479.
- [22] F. Johnson, *A general panel method for the analysis and design of arbitrary configurations in incompressible flow*, NASA Tech. Rep. NASA-CR-3079, National Tech. Inform. Service, Springfield, VA.
- [23] D. Lischinski, F. Rampieri, and D. P. Greenberg, *Discontinuity meshing for accurate radiosity*, IEEE Computer Graphics and Applications, 12(6):25-39, November 1992.
- [24] Yudell Luke, *The special functions and their approximations*, New York, Academic Press, 1969.
- [25] Michael F. Modest, *Radioactive Heat Transfer*, McGraw-Hill, Inc, 1993.
- [26] Ketan Mulmuley, *Computational Geometry: An Introduction through Randomized Algorithms*, Prentice Hall, 1998.
- [27] Y. Nievergelt and Y. Nievergelt, *Wavelets Made Easy*, Birkhauser Boston, 1999.
- [28] T. Nishita and E. Nakamae, *Continuous Tone Representation of Three Dimensional Objects taking account of Shadows and Interreflection*, Computer Graphics, 19(3), 23-30, 1985.
- [29] B. T. Phong, *Illumination for computer generated pictures*. Communications of the ACM, 18(6):311-317, June 1975.
- [30] F.P. Preparata and M.I. Shamos, *Computational Geometry-An Introduction*, Springer Verlag, New York, 1985.
- [31] J. O'Rourke, *Computational Geometry in C*, Cambridge University Press, 1994.
- [32] A. Rathsfeld, *Edge asymptotics for the radiosity equation over polyhedral boundaries*, Math. Methods Appl. Sci. 22 (1999), pp 217-241
- [33] D.F. Rogers, *Procedural Elements for Computer Graphics*, McGraw-Hill, New York, 1985.
- [34] H. Samet, *The Analysis and Design of Spatial Data Structures*, Addison-Wesley series in computer science, 1990.
- [35] P. Schröder and P. Harahan, *On the Form Factor between Two Polygons*, Computer Graphics(SIGGRAPH '93 Proceedings), vol.27, pp163-164.
- [36] P. Schröder, S. Gortler, M. Cohen, and P. Hanrahan. *Wavelet projections for radiosity*, In Proceedings of Fourth Eurographics Workshop on Rendering, pages 105-114, Eurographics, June 1993.
- [37] C.Schwab and W. Wendland, *On numerical cubatures of singular surface integrals in boundary element methods*, Numerische Mathematik, 62, 1992, Page 343-369.
- [38] Jaehoon Seol, *Analysis of the Radiosity Equation Using the Collocation Method*, PhD thesis, 2002, Univ. of Iowa, Iowa City.
- [39] M. Sonka, R. Boyle, V. Hlavac, R. Boyle, and V. Hlavac, *Image Processing, Analysis, and Machine Vision*, Brooks Cole Publishing Company, 1999.
- [40] J. Stoer and R. Bulirsch, *Introduction to Numerical Analysis*, Springer-Verlag, New York, 2001.
- [41] G. Strang and T. Nguyen, *Wavelets and Filter Banks*, Wellesley-Cambridge Press, 2000
- [42] A. Stroud, *Approximate Calculation of Multiple Integrals*, Prentice-Hall, New Jersey.
- [43] S. J.Teller, *Computing the Antipenumbra of an Area Light Source*, Computer Graphics, 26,2 July,1992.
- [44] S. Upstill, *The RenderMan<sup>TM</sup> Companion*, Addison-Wesley, Reading MA, 1989.
- [45] Alan Watt and Mark Watt, *Advanced Animation and Rendering Techniques*, ACM Press, 1992.
- [46] P. Wojtaszczyk, *A Mathematical Introduction to Wavelets*, Cambridge University Press, 1997.
- [47] Harold R. Zatz; *Galerkin Radiosity*, Proceedings of the 20th annual conference on Computer graphics, 1993, Pages 213 - 220.